photonics

MDPI

Article

Propagating and Evanescent TE-Polarized Bessel Light Beams in $\mathcal{PT}$-Symmetric Systems

Milena Dylko and Andrey Novitsky *

Faculty of Physics, Belarusian State University, Nezavisimosti Avenue 4, 220030 Minsk, Belarus; fiz.dylko@bsu.by
* Correspondence: novitsky@bsu.by

Abstract

Parity-time ($\mathcal{PT}$) symmetry offers a well-established route for enhancing light-matter interaction by means of formation of exceptional points. The model of plane waves is commonly used for finding and investigating exceptional points in open multilayer systems. Here we study behaviors of TE-polarized Bessel light beams in $\mathcal{PT}$-symmetric multilayer structures. It is shown that, due to the translational invariance of the planar interfaces, the exceptional and diabolic points of the Bessel beam are identical to those of a conventional plane wave with the same angle of incidence. Basing on this equivalence, we adopt the method of scattering matrices to TE-polarized non-paraxial Bessel beams and determine positions of exceptional points depending on the transverse wave number and non-Hermiticity parameter for both propagating and evanescent beams. We reveal the evolution of exceptional and diabolic lines when the number of layers changes and find their link to the transmission and reflection spectra. This research may pave the way for exploiting light beams in non-Hermitian photonics.

Keywords: scattering; Bessel light beam; $\mathcal{PT}$-symmetry; evanescent waves; exceptional point

1. Introduction

The parity-time ($\mathcal{PT}$)-symmetric system as a sort of a non-Hermitian system was first introduced more than two decades ago within the framework of quantum mechanics [1,2] and has since enabled the exploration of numerous remarkable effects in optics, such as unidirectional invisibility [3,4], simultaneous coherent perfect absorption and lasing (CPA laser) [5–8], asymmetric optical pulling and pushing forces [9], phase transitions between regimes of coherent amplification and absorption [10], enhanced photonic spin Hall effect near exceptional points [11], and so on.

$\mathcal{PT}$-symmetric systems are inherently non-Hermitian, which manifests itself through the properties of either Hamiltonian $\hat{H}$ or scattering matrix $\hat{S}$ [7,12,13]. In particular, for nonmagnetic optical media, the $\mathcal{PT}$-symmetry dictates accomplishment of the condition $\varepsilon(\mathbf{r}) = \varepsilon^*(-\mathbf{r})$ [3], which is most commonly implemented in structures composed of alternating layers of equal thickness $d_1 = d_2 = d$ with opposite signs of the imaginary part of the dielectric permittivity as $\mathrm{Im}(\varepsilon_1) = -\mathrm{Im}(\varepsilon_2)$. A distinctive feature of such systems is a possibility of spontaneous $\mathcal{PT}$ symmetry breaking at an exceptional point (EP) defined by coalescing eigenvalues and eigenvectors of the scattering matrix or Hamiltonian [13–16]. The topological nature of these transitions is intimately related to EPs inducing unique phenomena such as eigenmode exchange and phase jumps in reflection coefficients [17]. For propagating waves, the eigenvalues of the scattering matrix S must be unimodular as $|s_1| = |s_2| = 1$ in the $\mathcal{PT}$-symmetric regime, whereas the eigenvalues are reversed as

Check for updates

Received: 6 August 2026
Revised: 7 September 2026
Accepted: 8 September 2026
Published: 10 September 2026

Copyright: © 2026 by the authors. Licensee MDPI, Basel, Switzerland. This article is an open access article distributed under the terms and conditions of the Creative Commons Attribution (CC BY) license.

$|s_1| = 1/|s_2|$ in the $\mathcal{PT}$-symmetry broken regime, the eigenstates being amplified and attenuated [7]. Evanescent waves exhibit an alternative means for insightful analysis of the $\mathcal{PT}$-symmetry through tailoring the transverse wave-vector component as an additional parameter governing the $\mathcal{PT}$-symmetric state of the system [18–20]. It must be noted, that no unique definition of the scattering matrix exists when it is introduced independently of system's Hamiltonian [21]. However, analyzing the $\mathcal{PT}$-symmetric multilayer structure directly allows us to investigate phase transitions for any scattering matrix that describes such a system without relating it to the Hamiltonian. Since the scattering matrix relates the amplitudes of incoming and outgoing waves, there is a certain freedom in choosing an order of these amplitudes and, accordingly, in defining the scattering matrix itself. In this work, we consider two such definitions, S_1 and S_2, where the first of them is more convenient for predicting the lasing threshold, while the second one better corresponds to the $\mathcal{PT}$-symmetric Hamiltonian [15,21].

A plane wave has traditionally been a regular object for studying $\mathcal{PT}$ symmetry and has enabled the investigation of numerous physical phenomena [3,7,22], with many more yet to be discovered. While $\mathcal{PT}$-symmetric phase transitions and exceptional points have been extensively studied for plane waves, recent breakthroughs demonstrate that structured light fields fundamentally alter scattering dynamics in non-Hermitian media [23–26]. However, another tool in the context of $\mathcal{PT}$ symmetry, a Bessel beam [27,28], has received comparatively little attention, particularly evanescent beams [19,29,30].

Bessel beams are nondiffracting solutions of the wave equation in cylindrical coordinates, formed by a superposition of plane waves whose wave vectors lie on the surface of a cone with half-cone angle θ [27]. Due to their wavefront, they inherently exhibit rich polarization structure, including $s-$, $p-$, transverse, and longitudinal polarizations [31]. The transverse wave-vector component $k_t = kq$ determines the beam profile as shown in Figure 1. For $q < 1$ the beam is propagating; for $q > 1$, the wave-vector cone becomes imaginary, and the beam transitions into the evanescent regime, characterized by oscillations in the transverse direction and exponential decay along the propagation axis [19]. Although numerous studies have investigated the properties and applications of paraxial and nonparaxial Bessel beams [31–35], the relatively unexplored combination of evanescent Bessel beams with $\mathcal{PT}$ symmetry as a scientific research is missing.

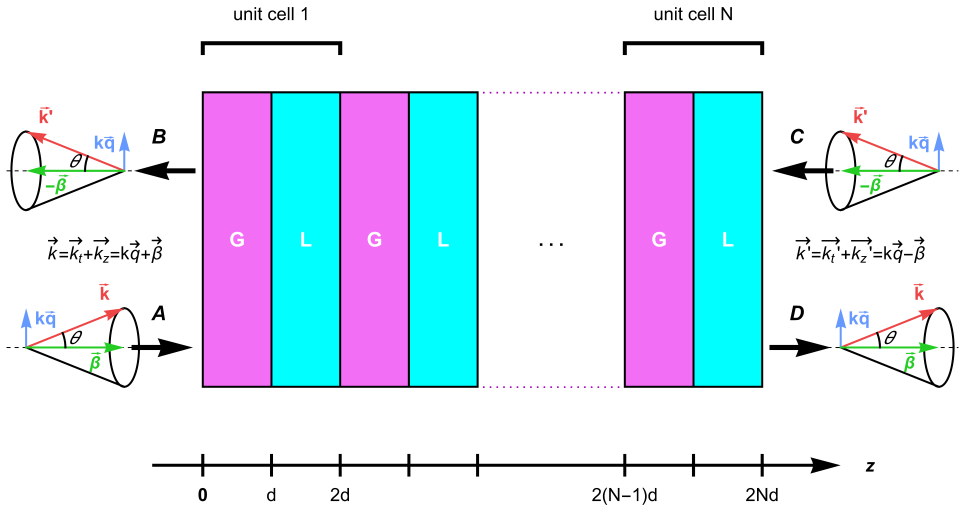


Figure 1. A sketch of the multilayer structure of total thickness $2Nd$ consisting of layers with gain labeled by the letter G and layers with loss labeled by the letter L. A, D and B, C denote the amplitudes of the forward and backward Bessel beams, respectively.

For this reason, the main aim of this work is to construct scattering matrices for both propagating and evanescent nonparaxial TE-polarized Bessel beams, thereby providing a quantitative investigation of the $\mathcal{PT}$-symmetry with this class of fields. This formalism is essential for mapping the evolution of $\mathcal{PT}$-symmetric systems, bridging the gap between fundamental non-Hermitian physics and structured-light applications in sensing and photonics.

Accordingly, in Section 2 we introduce the system under study and the method for constructing the scattering matrices of a Bessel beam; in Section 3 we discuss the obtained results for the two types of scattering matrices as functions of the tunable system parameters; in Section 4 we sum up the obtained results.

2. Methods

Basing on the matrix method proposed in [32], here we will establish the form of the scattering matrix of a Bessel beam interacting with a planar layered system. To this end, we consider the multilayer nonmagnetic structure shown in Figure 1 placed in an air with the dielectric permittivity $\varepsilon_0 = 1$. The $\mathcal{PT}$-symmetric structure have to consist of alternating layers of the same thickness $d_G = d_L = d$ with gain and loss described by the complex dielectric permittivity $\varepsilon_G = \varepsilon' - i\varepsilon''$ and $\varepsilon_L = \varepsilon' + i\varepsilon''$, respectively. A couple of such slabs forms a unit cell, the number of unit cells N in the system being a variable. Let us consider a monochromatic Bessel beam of the order m propagating along the z-axis incident onto the multilayer system. According to [32], its electric and magnetic field strengths in a medium of permittivity ε read as

$$\begin{aligned} \mathbf{E} &= e^{im\varphi+i\beta z}\left(J_m(kqr)c_2\mathbf{e}_z - \frac{1}{q}c_1(\mathbf{e}_z\times\mathbf{b}) + \frac{\beta}{kq}c_2\mathbf{b}\right), \\ \mathbf{H} &= e^{im\varphi+i\beta z}\left(J_m(kqr)c_1\mathbf{e}_z + \frac{\beta}{kq}c_1\mathbf{b} + \frac{\varepsilon}{q}c_2(\mathbf{e}_z\times\mathbf{b})\right), \end{aligned} \tag{1}$$

where z is the beam propagation direction, (r, φ, z) are the cylindrical coordinates, c_1 and c_2 are complex constants, $J_m(x)$ is the m-th order Bessel function of the first kind, $k = 2\pi/\lambda$ is the wavenumber in vacuum, λ is the wavelength, $q = k_t/k = \sin\theta$ is the normalized transverse wavenumber, θ is the half-cone angle of the Bessel beam shown in Figure 1, $\beta = k\sqrt{\varepsilon - q^2}$ is the longitudinal wave number, and

$$\mathbf{b} = iJ_m'(kqr)\mathbf{e}_r - \frac{m}{kqr}J_m(kqr)\mathbf{e}_\varphi, \qquad J_m'(kqr) = \frac{dJ_m}{d(kqr)}.$$

Since the translational invariance of the multilayer structure conserves the transverse wavenumber q, the lateral distribution of the Bessel beam does not affect the boundary conditions at the planar interfaces, making the amplitude matching mathematically identical to that of a single plane wave. Further we consider the case of a TE-polarized Bessel beam ($c_2 = 0$). The total field inside the multilayer structure is formed by the superposition of forward- and backward- propagating waves, characterized by complex amplitudes. Thus, the transverse components (with respect to the z axis) of the electric and magnetic fields can then be derived from Equation (1) as

$$\begin{aligned} \mathbf{E}_\perp &= -\frac{1}{q}e^{im\varphi}\left(c_1'e^{i\beta z} + c_1''e^{-i\beta z}\right)(\mathbf{e}_z\times\mathbf{b}), \\ \mathbf{H}_\perp &= \frac{\beta}{kq}e^{im\varphi}\left(c_1'e^{i\beta z} - c_1''e^{-i\beta z}\right)\mathbf{b}, \end{aligned}$$

where c_1' and c_1'' are the amplitudes of the forward and backward propagating Bessel beams, respectively. The magnitudes of transverse electric $\mathbf{E}_\perp = E_\perp \mathbf{e}_z \times \mathbf{b}$ and magnetic $\mathbf{H}_\perp = H_\perp \mathbf{b}$ fields can be expressed in terms of amplitudes c_1' and c_1'' as

$$\begin{pmatrix} E_\perp(z) \\ H_\perp(z) \end{pmatrix} = P(z) \begin{pmatrix} c_1' \\ c_1'' \end{pmatrix}, \qquad P(z) = e^{im\phi} \begin{pmatrix} -\frac{1}{q} e^{i\beta z} & -\frac{1}{q} e^{-i\beta z} \\ \frac{\beta}{kq} e^{i\beta z} & -\frac{\beta}{kq} e^{-i\beta z} \end{pmatrix}. \tag{2}$$

Following its definition, the scattering matrix relates the amplitudes of outgoing waves to those of incoming ones. Therefore, our objective is to relate the tangential fields at the starting point $z = 0$ with those at the final point $z = 2Nd$ for any number of unit cells N and thickness of the single cell $2d$ using the matrix representation given by Equation (2). The transverse field components at two boundaries of the multilayer are related by the transfer matrix Θ_0^z as follows [32]

$$\begin{pmatrix} E_\perp(z) \\ H_\perp(z) \end{pmatrix} = \Theta_0^z \begin{pmatrix} E_\perp(0) \\ H_\perp(0) \end{pmatrix}, \qquad \Theta_0^z = P(z)P^{-1}(0) = \begin{pmatrix} \cos\beta z & -i\frac{k}{\beta}\sin\beta z \\ -i\frac{\beta}{k}\sin\beta z & \cos\beta z \end{pmatrix}.$$

In the considered structure, the Bessel beam passes through the gain and loss layers within a single unit cell. Consequently, the transfer matrix of the unit cell is a product of the transfer matrices of each layer of the same thickness:

$$[\Theta_0^d]_L [\Theta_0^d]_G = \begin{pmatrix} \cos\beta_L d & -i\frac{k}{\beta_L}\sin\beta_L d \\ -i\frac{\beta_L}{k}\sin\beta_L d & \cos\beta_L d \end{pmatrix} \begin{pmatrix} \cos\beta_G d & -i\frac{k}{\beta_G}\sin\beta_G d \\ -i\frac{\beta_G}{k}\sin\beta_G d & \cos\beta_G d \end{pmatrix}, \tag{3}$$

where the subscripts $i = G, L$ denote the gain or loss media and the longitudinal wavenumber is given by $\beta_i = k\sqrt{\varepsilon_i - q^2}$. The total transfer matrix of N cells is obtained by raising the matrix described by Equation (3) to the N-th power:

$$\begin{pmatrix} E_\perp(2Nd) \\ H_\perp(2Nd) \end{pmatrix} = \Theta_{tot} \begin{pmatrix} E_\perp(0) \\ H_\perp(0) \end{pmatrix} = ([\Theta_0^d]_L [\Theta_0^d]_G)^N \begin{pmatrix} E_\perp(0) \\ H_\perp(0) \end{pmatrix}.$$

Figure 1 shows the amplitudes of the Bessel beams on the left and right sides of the multilayer structure, propagating along the z axis (A and D) and in the opposite direction (B and C). Expressing the field components in terms of the introduced amplitudes $(D, C)^T$ at $z = 2Nd$ and $(A, B)^T$ at $z = 0$ using Equation (2), we arrive at

$$\begin{pmatrix} E_\perp(2Nd) \\ H_\perp(2Nd) \end{pmatrix} = P_0(2Nd) \begin{pmatrix} D \\ C \end{pmatrix}, \qquad \begin{pmatrix} E_\perp(0) \\ H_\perp(0) \end{pmatrix} = P_0(0) \begin{pmatrix} A \\ B \end{pmatrix},$$

where the subscript 0 in the matrices $P_0(2Nd)$ and $P_0(0)$ denotes the ambient medium and superscript T stands for the transpose. As a result, the amplitudes on the right-hand side of the multilayer system are related to those on the left-hand side as

$$\begin{pmatrix} D \\ C \end{pmatrix} = M \begin{pmatrix} A \\ B \end{pmatrix}, \qquad M = P_0^{-1}(2Nd)\Theta_{tot}P_0(0). \tag{4}$$

The scattering matrix relates the outgoing amplitudes to the incoming ones as [15]

$$\begin{pmatrix} B \\ D \end{pmatrix} = S_1 \begin{pmatrix} A \\ C \end{pmatrix}, \qquad S_1 = \begin{pmatrix} r_L & t \\ t & r_R \end{pmatrix}, \tag{5}$$

where $r_L = r_{LR}$ and $t = t_{LR}$ ($r_R = r_{RL}$ and $t = t_{RL}$) are the complex field reflection and transmission coefficients for the wave incident from the left (right) to the right (left). Using Equation (4), we determine the amplitudes B and D by means of A and C and get the following expression for the scattering matrix S_1:

$$S_1 = \frac{1}{M_{22}} \begin{pmatrix} -M_{21} & M_{11}M_{22} - M_{12}M_{21} \\ 1 & M_{12} \end{pmatrix}.$$

Condition $\det M = 1$ [15] allows us to rewrite the matrix S_1 in a simpler form

$$S_1 = \frac{1}{M_{22}} \begin{pmatrix} -M_{21} & 1 \\ 1 & M_{12} \end{pmatrix}.$$

Scattering matrix S_2 relates the switched outcomming amplitudes according to

$$\begin{pmatrix} D \\ B \end{pmatrix} = S_2 \begin{pmatrix} A \\ C \end{pmatrix}, \qquad S_2 = \begin{pmatrix} t & r_R \\ r_L & t \end{pmatrix} \tag{6}$$

and can be expressed in terms of the matrix S_1 as

$$S_2 = \begin{pmatrix} 0 & 1 \\ 1 & 0 \end{pmatrix} S_1 = \frac{1}{M_{22}} \begin{pmatrix} 1 & M_{12} \\ -M_{21} & 1 \end{pmatrix}.$$

The eigenvalues of the matrix S_1 can be expressed by means of the complex field reflection and transmission coefficients as

$$s_{1,2}^{(1)} = \frac{r_L + r_R}{2} \pm \sqrt{\left(\frac{r_L - r_R}{2}\right)^2 + t^2},$$

and by means of the matrix M components as

$$s_{1,2}^{(1)} = \frac{M_{12} - M_{21} \pm \sqrt{(M_{12} + M_{21})^2 + 4}}{2M_{22}}.$$

The condition for the emergence of EPs corresponds to the coalescence of both eigenvalues and eigenvectors, which for the matrix S_1 requires

$$(M_{12} + M_{21})^2 + 4 = 0. \tag{7}$$

The eigenvalues of the matrix S_2 are expressed as

$$s_{1,2}^{(2)} = t \pm \sqrt{r_L\, r_R},$$

or, alternatively, as

$$s_{1,2}^{(2)} = \frac{1 \pm \sqrt{-M_{12}M_{21}}}{M_{22}}.$$

For the matrix S_2 eigenvalues, the EP condition is

$$M_{12}M_{21} = 0, \tag{8}$$

with the additional requirement that either M_{12} or M_{21} vanishes, but not both of them simultaneously. Otherwise, the matrix S_2 becomes proportional to the identity matrix, and the eigenvalue degeneracy corresponds to a diabolic point (DP) rather than an EP.

3. Results

First of all, we are interested in studying eigenvalues of the scattering matrix for both propagating and evanescent TE-polarized Bessel beams to determine the state of the system in the context of available $\mathcal{PT}$ symmetry. The real part of the dielectric permittivity of layers in the unit cell is taken as $\varepsilon' = 2$ and the radiation wavelength is set to $\lambda = 1000$ nm. The dependence on the following key parameters affecting $\mathcal{PT}$ symmetry is studied: (i) the imaginary part of the dielectric permittivity ε'' and (ii) the value of the normalized transverse wavevector component q that determines the wave propagation regime (propagating Bessel beam for $q < 1$ and evanescent beam for $q > 1$). Propagating and evanescent beams are defined in the ambient medium being the beams incident on the multilayer system. The parameter space of ε'' and q is used to determine the regions of $\mathcal{PT}$-symmetric and $\mathcal{PT}$ symmetry broken states and their transformation when the layer thickness d and the number of unit cells N changes. It should also be noted that the scattering matrices given by Equations (5) and (6) are independent of the integer azimuthal number m of the Bessel beam. As a Bessel beam can be represented as a coherent superposition of plane waves whose wavevectors form a cone with a half-angle θ determined by the normalized transverse wavenumber $q = \sin\theta$, the interaction of a plane wave with a planar interface depends solely on its angle of incidence, polarization, and the material parameters, but is completely independent of the azimuthal orientation of its wavevector. Since all plane-wave components of the Bessel beam share the identical incident angle θ and TE-polarization, they undergo exactly the same reflection and transmission processes. The azimuthal number m governs the transverse spatial distribution of the field and its orbital angular momentum, but it does not affect the local boundary conditions at the planar interfaces. Due to the translational invariance of the multilayer structure in the transverse plane, the reflection and transmission coefficients depend only on structure's parameters and q, remaining identical for all plane-wave components regardless of their azimuthal angle ϕ. Consequently, the eigenvalues of the scattering matrix and the conditions for $\mathcal{PT}$ symmetry breaking are independent of the beam order m.

In Figure 2, we show the behavior of the absolute difference in the moduli of S_1-matrix eigenvalues $|s_{1,2}|$ while varying the aforementioned parameters q and ε'' for the fixed number of unit cells $N = 1$. In the density plots, the colored regions exhibit non-zero values of the absolute difference and define the $\mathcal{PT}$ symmetry broken regions. The blue lines are the EP lines determined by Equation (7) and separating the $\mathcal{PT}$-symmetric and $\mathcal{PT}$ symmetry broken phases. The black regions attached to the EP lines are $\mathcal{PT}$-symmetric with equal moduli of the eigenvalues $|s_1| = |s_2|$. For the layer thicknesses $d = 75$ nm in Figure 2a and $d = 125$ nm in Figure 2b, the EP lines between the colored and black regions are absent at $q < 1$. The increase in the layer thickness results in broadening the region of the great values of the difference $||s_1| - |s_2||$ in the range from $\varepsilon'' \approx 2.5$ to $\varepsilon'' \approx 3.7$, thus, narrowing the black-colored domain. This means that the black-colored region is not characterized by equal absolute eigenvalues, but rather demonstrates the gradual decrease of $||s_1| - |s_2||$. For $q > 1$, there exist $\mathcal{PT}$-symmetric regions in which the eigenvalue moduli are equal as $|s_1| = |s_2|$, but not equal to the unity. Increasing the layer thickness d leads to reduction of the $\mathcal{PT}$ symmetry broken region and, consequently, allows one to avoid a precise tuning of parameters ε'' and $q > 1$ to observe $\mathcal{PT}$-symmetric states for evanescent Bessel beams experimentally. It should also be noted that the white region in both plots in the range from $q = 1$ to $q \approx 1.17$, associated with the excitation of an eigenmode upon transition to the evanescent regime, corresponds to the growth of the only eigenvalue. To understand the relationship between the layer thickness d and the number of unit cells N, we invoke the Bloch band theory for periodic structures. The transfer matrix of a single unit cell is characterized by the phase accumulated within the gain and loss layers, which

is proportional to $\Phi = \beta d$. For N unit cells, the total transfer matrix is the N-th power of the unit cell matrix. That is why its eigenvalues depend on the accumulated phase $N\Phi$. The full matrix M accounts for both this internal phase and the phase accumulated in the ambient medium $\beta_0 2Nd$. Varying N and d influence similarly, because both scale the total phase that dictates the interference and resonance conditions within the periodic structure. As the total phase wraps around while increasing d, new resonance conditions are met, leading to the emergence of additional EPs and more complex $\mathcal{PT}$-symmetric regions.

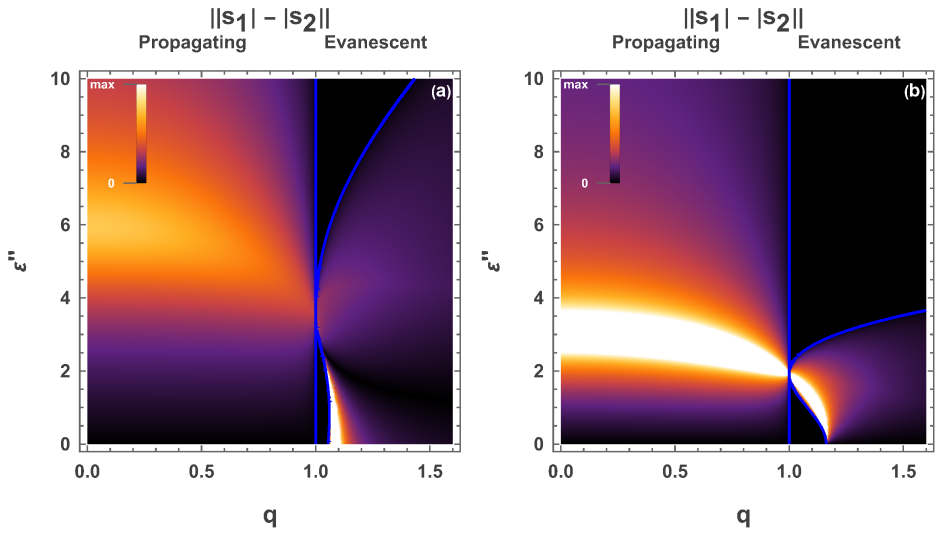


Figure 2. Absolute difference in the moduli of S_1-matrix eigenvalues $|s_{1,2}|$ for the single unit cell ($N = 1$), if the layer thickness equals (**a**) $d = 75$ nm and (**b**) $d = 125$ nm. The EP lines are marked in blue.

This behavior is illustrated in Figure 3, which shows the change in the absolute difference $||s_1| - |s_2||$ when varying the number of unit cells N at fixed $d = 125$ nm. The plot for the number of cells $N = 1$ depicted in panel (a) has been already discussed above as Figure 2b showing no EPs in the case of propagating Bessel beams. Upon the transition to a couple of unit cells $N = 2$, we notice the emergence of $\mathcal{PT}$-symmetric and $\mathcal{PT}$ symmetry broken phases sharply detached one from another for both propagating and evanescent waves. We can conclude that only starting from $N = 2$ it is possible to identify a $\mathcal{PT}$-symmetric phase for propagating beams in the case of the scattering matrix S_1. In general, $\mathcal{PT}$ symmetry broken ($\mathcal{PT}$-symmetric) phase is observed for the great non-Hermiticity parameters ε'' and propagating (evanescent) Bessel beams independently of N. The number of $\mathcal{PT}$-symmetric regions M changes at every even number of unit cells $N_e = 2, 4, 6, 8$ for propagating and evanescent Bessel beams according to the relationship $M = N_e/2$. For the odd number of unit cells and evanescent Bessel beams, it always exists a region of $\mathcal{PT}$-symmetric phase at small ε'' and q near 1. So far the distinct behavior observed for even and odd N in Figure 3 is a direct consequence of the specific parameter choice. The condition for the occurrence of EPs across the studied region is satisfied at $d \approx 250$ nm, which is equivalent to $N = 2$ unit cells at $d = 125$ nm. Since the accumulated phase is periodic, an odd number of unit cells corresponds to an intermediate phase that does not satisfy this specific resonance condition, whereas an even number of cells does. Thus, this parity-dependent difference in the phase diagrams is specific to the chosen thickness and number of unit cells, rather than a universal feature of the system.

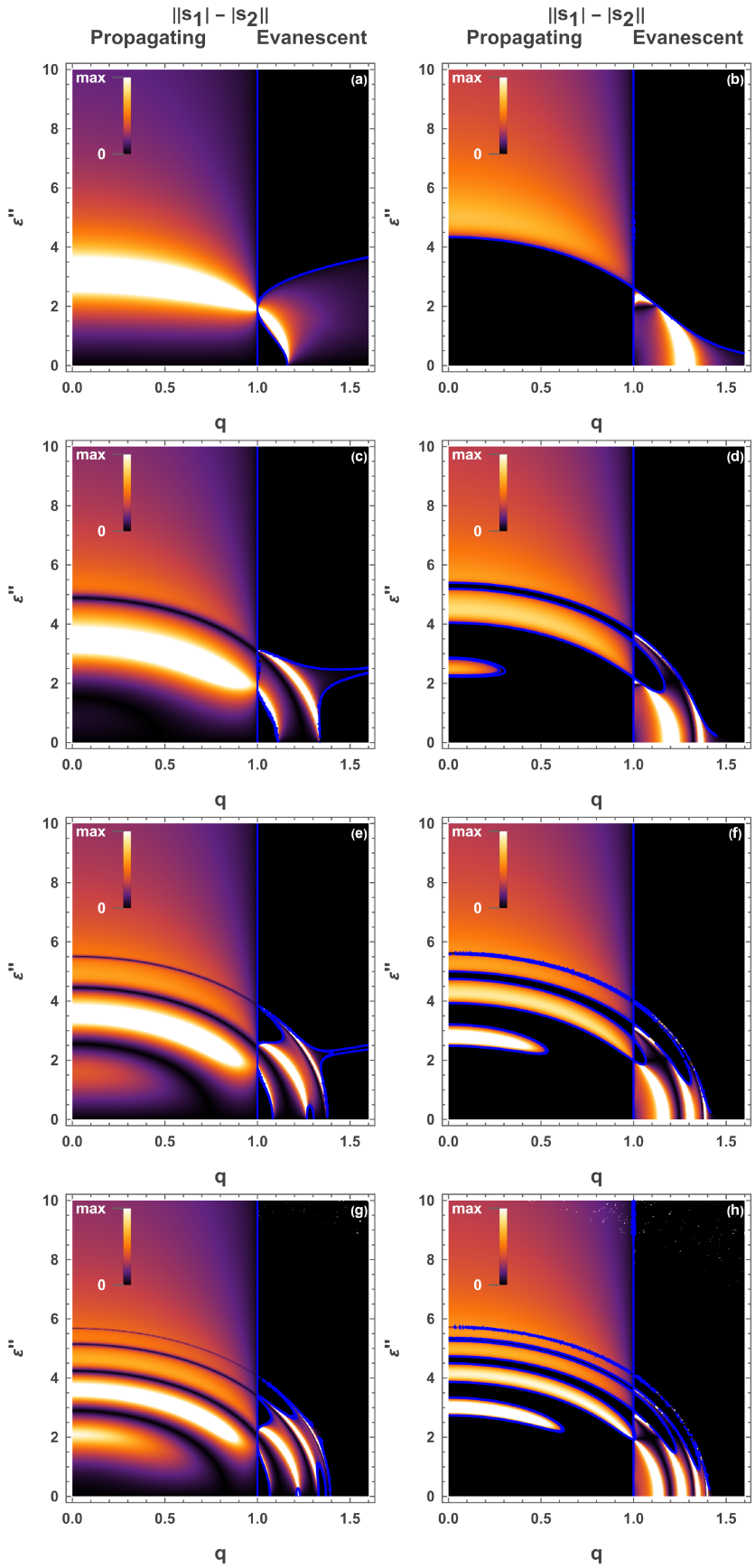


Figure 3. Absolute difference in the moduli of S_1-matrix eigenvalues $|s_{1,2}|$ for the layer thickness $d = 125$ nm and varying number of unit cells: (**a**) $N = 1$, (**b**) $N = 2$, (**c**) $N = 3$, (**d**) $N = 4$, (**e**) $N = 5$, (**f**) $N = 6$, (**g**) $N = 7$, (**h**) $N = 8$. The EP lines are marked in blue.

It must be noted that at large N and $q > 1$, the longitudinal wavenumber becomes imaginary, introducing exponentially growing terms into the transfer matrix. In addition, at $q = 1$, the boundary matrix P_0^{-1} becomes singular. These features require careful numerical treatment to avoid instabilities and ensure continuous transition from the propagating to evanescent regime. One may need to employ analytical techniques at singular points and enhancement of numerical precision for mitigating error accumulation in matrix operations.

So far, we have considered the eigenvalues of the scattering matrix S_1. However, based on the fact that there is a certain freedom in defining the scattering matrix, we also investigate the eigenvalues of the matrix S_2, defined by Equation (6).

Figure 4a shows the domains of $\mathcal{PT}$-symmetric and $\mathcal{PT}$ symmetry broken states of the scattering matrix S_2 for the layer thickness $d = 75$ nm and number of unit cells $N = 1$, separated by a blue EPs line defined by Equation (8). It is obvious that, in contrast to the eigenvalues of the matrix S_1 depicted in Figure 2a at the same system parameters, there exists a well-defined $\mathcal{PT}$-symmetric phase with the unimodular eigenvalues $|s_1| = |s_2| = 1$ for the propagating Bessel beams, while the region of evanescent beams, on the contrary, corresponds to the $\mathcal{PT}$ symmetry broken phase. To continue studying the phase diagram, we now turn to the effects that occur when the number of unit cells N increases. First noticeable changes arise at $N = 3$. As it is shown in Figure 4b, for $q < 1$, an additional line of eigenvalues' degeneracy points (the green line number 3) appears in the parameter space of ε'' and q, where $\mathcal{PT}$ symmetry phase transition does not take place. That is, the line 3 is composed of DPs. At the same time, the evanescent beams remain completely in the $\mathcal{PT}$ symmetry broken phase. With the further increase in the number of unit cells, the new degeneracy lines (green lines) emerge, and the previous lines shift. It is important to note that this rule applies only to the eigenvalue degeneracy lines, but not to the blue EP lines that do not change their position in the considered parameter space. This tendency is shown for $N = 5$ in Figure 4c, where the eigenvalues' degeneracy line 3 present in Figure 4b extends into the evanescent region along with the appearance of another line 4 in the propagating region. Despite the appearance of a black region at $q > 1$, which may look like $\mathcal{PT}$-symmetric one, the evanescent region still remains in the $\mathcal{PT}$ symmetry broken phase. This assertion is confirmed by the absence of blue lines of the $\mathcal{PT}$ symmetry phase transition. The absolute difference in the eigenvalue moduli tends to zero in this region, but it is not equal to zero.

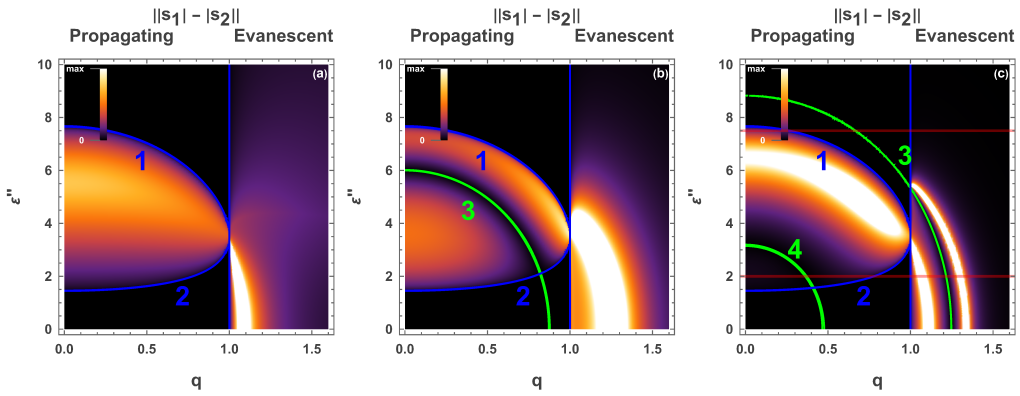


Figure 4. Absolute difference in the moduli of S_2-matrix eigenvalues $|s_{1,2}|$ for the layer thickness $d = 75$ nm and vatious number of unit cells: (**a**) $N = 1$, (**b**) $N = 3$, and (**c**) $N = 5$. The EP and DP lines are marked in respectively blue and green.

To clarify the eigenvalue behavior in black regions of Figure 4c, we examine the eigenvalue moduli of the scattering matrix S_2 for the same layer thickness $d = 75$ nm and number of unit cells $N = 5$, but different non-Hermiticity parameters ε'' as shown in Figure 5.

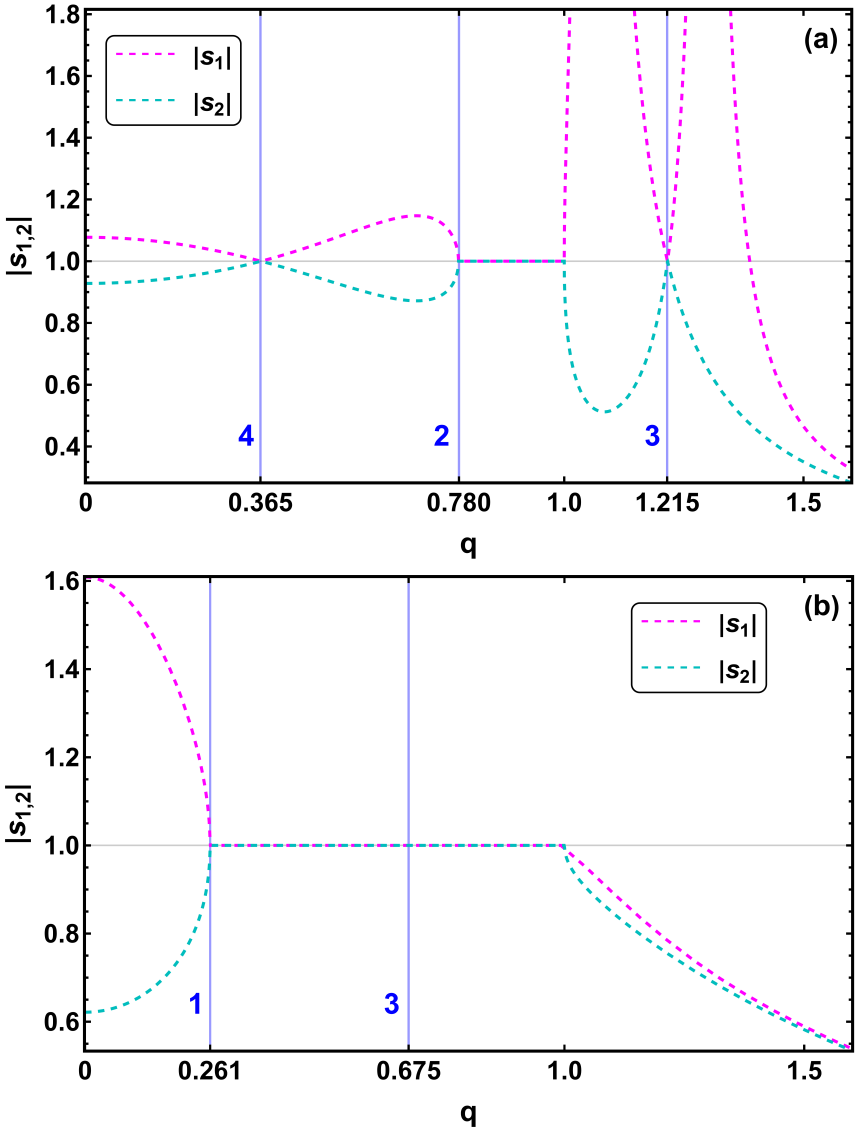


Figure 5. Absolute eigevalues $|s_{1,2}|$ of the matrix S_2 for the thickness $d = 75$ nm, number of unit cells $N = 5$, and (**a**) $\varepsilon'' = 2$ and (**b**) $\varepsilon'' = 7.5$. Vertical lines correspond to the positions of exceptional (1 and 2) and diabolic (3 and 4) points.

Figure 5a depicts the absolute eigenvalues for $\varepsilon'' = 2$ and propagating Bessel beams ($q < 1$). In this case, the system stays in the $\mathcal{PT}$ symmetry broken phase up to the EP at $q \approx 0.780$, beyond which it undergoes a phase transition. In Figure 4c, the EP is recognized by the abrupt color change when transition through the blue EP line occurs. The point $q = 0.365$ is a point of eigenvalue degeneracy, where eigenvalues exchange their behaviors. However, this point does not alter the phase, since eigenvectors are not degenerate (diabolic point). A similar situation is observed for evanescent beams ($q > 1$), where, as mentioned earlier, the eigenvalues in the $\mathcal{PT}$ symmetry broken phase are unequal. One more diabolic point that does not vary the phase can be noticed at $q \approx 1.215$. With further increase in the normalized transverse wavevector component q, the eigenvalue moduli tend toward each other but cannot become equal at finite parameters q. Thus, for evanescent Bessel beams,

the system keeps the $\mathcal{PT}$ symmetry broken phase despite the presence of the eigenvalue degeneracy point. In Figure 5b, we investigate the behavior of the eigenvalue moduli $|s_{1,2}|$ for the greater value of the parameter $\varepsilon'' = 7.5$. In the region of propagating Bessel beams, the point $q \approx 0.261$ is an EP, ensuring the phase transition from the $\mathcal{PT}$-broken to symmetric state. The eigenvalue moduli for evanescent beams, as in the case of the lower non-Hermiticity parameter in Figure 5a, asymptotically tend to merge, indicating a $\mathcal{PT}$ symmetry broken state of the system, which cannot be clearly grasped from Figure 4c.

Appearance of the phase transition between $\mathcal{PT}$-symmetric and $\mathcal{PT}$ symmetry broken phases can be better understood from Figure 6 showing the logarithms of the transmittance $\ln T = \ln |t|^2$ in Figure 6a,a′, reflectance to the right $\ln R_R = \ln |r_R|^2$ in Figure 6b,b′, and reflectance to the left $\ln R_L = \ln |r_L|^2$ in Figure 6c,c′ for the layer thickness $d = 75$ nm.

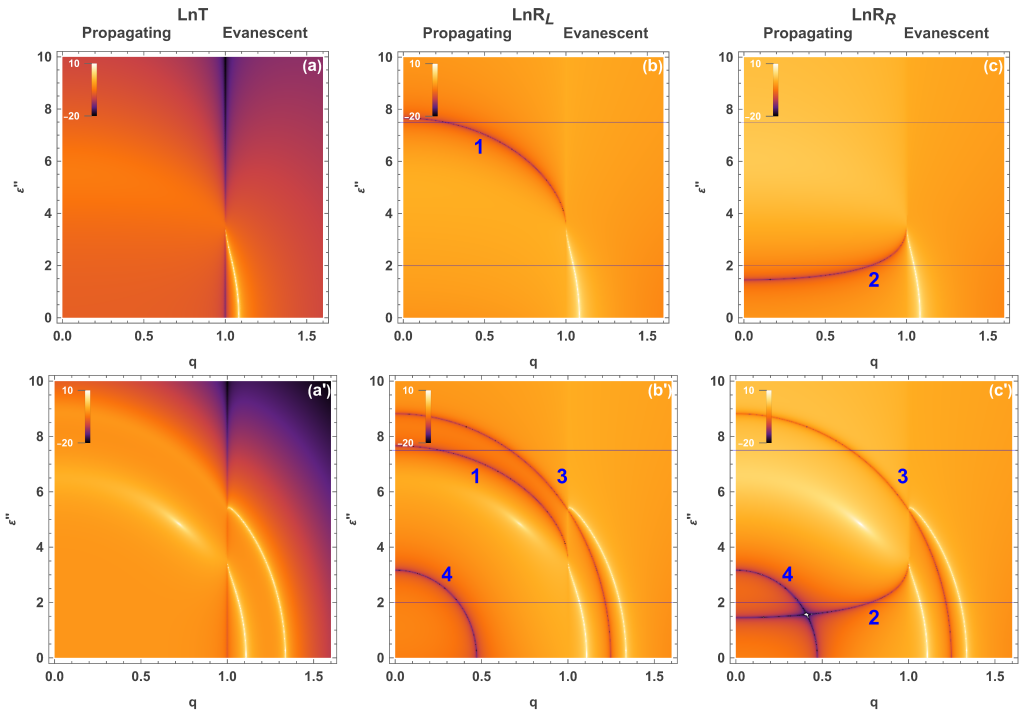


Figure 6. Logarithms of (**a**,**a′**) transmittance $\ln T$, (**b**,**b′**) reflectance to the right $\ln R_R$, and (**c**,**c′**) reflectance to the left $\ln R_L$ for the layer thickness $d = 75$ nm; panels (**a**–**c**) and (**a′**–**c′**) correspond to the number of unit cells $N = 1$ and $N = 5$, respectively.

Despite the fact that the transmission t and reflection r_R, r_L coefficients define both S_1 and S_2 matrices, they are able to predict the $\mathcal{PT}$-symmetric phase transitions in the chosen parameter space following exclusively from the definition of matrix S_2 and its eigenvalues given by Equation (2). The coalescence $s_1 = s_2$ occurs only if $r_L r_R = 0$, meaning that at least one of the reflection amplitudes vanishes. Consequently, the EPs and diabolic degeneracies of S_2 physically manifest themselves as respectively anisotropic transmission and perfect transmission resonances. In contrast, for the matrix S_1, the eigenvalue degeneracy condition shown by Equation (2) requires $t = 0$ and $r_L = r_R$, which corresponds to the regime of total reflection. The dark lines in Figure 6 represent the zero value of the corresponding quantity. The only dark lines at $q = 1$ in the plots of $\ln T$ [panels (a) and (a′)] are related to the transition from the propagating to evanescent regime, which is also distinguishable in Figure 4a for the S_2 matrix. Figure 6a–c show the logarithms of the transmittance and reflectances for the number of cells $N = 1$. The only bright line in all three plots for the transmittance and reflectances [panels (a), (b) and (c)] defines the excitation of an eigenmode at $q > 1$. The horizontal lines $\varepsilon'' = 2$ and $\varepsilon'' = 7.5$ [panels (b), (c), (b′), and (c′)] correspond to Figure 5a and 5b, respectively. Vertical blue lines in Figure 5 mark the values

of q at which the reflections are minimal. Thus, the dark lines 1 and 2 in Figure 6b,c are the EP lines in the parameter space of ε'' and q. They can be also noticed in Figure 4a. In the case of the number of cells $N = 5$ [panels (a′), (b′) and (c′) in Figure 6], the dark lines numbered 1 and 2 are again the EP lines describing the $\mathcal{PT}$ symmetry phase transition. However, the lines 3 and 4 emerging simultaneously in two plots are the lines of eigenvalue degeneracy that are not accompanied by the phase transition. Thus, the vanishing of the single reflectance, $R_L = 0$ or $R_R = 0$, is the criterion of the $\mathcal{PT}$ symmetry phase transition for the S_2 matrix, whereas when $R_L = R_R = 0$, the eigenvalues of the scattering matrix degenerate, but the eigenvectors do not; that is, an EP is not formed.

To illustrate the distinction between EPs and DPs through the behavior of complex reflection and transmission amplitudes, in Figure 7, we show the moduli [panel (a)] and arguments [panel (b)] of r_R, r_L, and t while varying q at fixed $d = 75$ nm, $\varepsilon'' = 2$ and $N = 5$. At the point number 4 with $q = 0.365$, the moduli of both reflection amplitudes $|r_R|$ and $|r_L|$ simultaneously approach to zero, while the transmission modulus $|t|$ reaches unity, corresponding to the bidirectional reflectionless scattering. As depicted in Figure 7b, the arguments of r_R and r_L both exhibit a sharp jump from $\pi/2$ to $-\pi/2$ when crossing this point, whereas the phase of t varies without any discontinuity. We quantify the degree of the eigenvector coalescence by computing their overlap, defined as the absolute value of the normalized inner product of the two eigenvectors $|\langle v_1|v_2\rangle|/(\|v_1\|\|v_2\|)$. The overlap of S_2 eigenvectors at this point is equal to 0.623, confirming that the eigenvectors remain linearly independent. This simultaneous vanishing of both reflection amplitudes corresponds to $M_{12} = M_{21} = 0$, which renders the scattering matrix S_2 proportional to the identity matrix and thus diagonalizable, confirming that this degeneracy is a DP. At the point number 2 with $q = 0.780$, only $|r_R|$ vanishes, while $|r_L|$ remains finite and $|t| = 1$, corresponding to unidirectional reflectionless scattering. Only the phase of r_R exhibits a jump of π at this point, while the arguments of r_L and t vary without any abrupt behavior. The eigenvector overlap reaches 1.00, confirming the coalescence of both eigenvalues and eigenvectors and non-diagonalizable nature of the matrix S_2, making the point number 2 an EP.

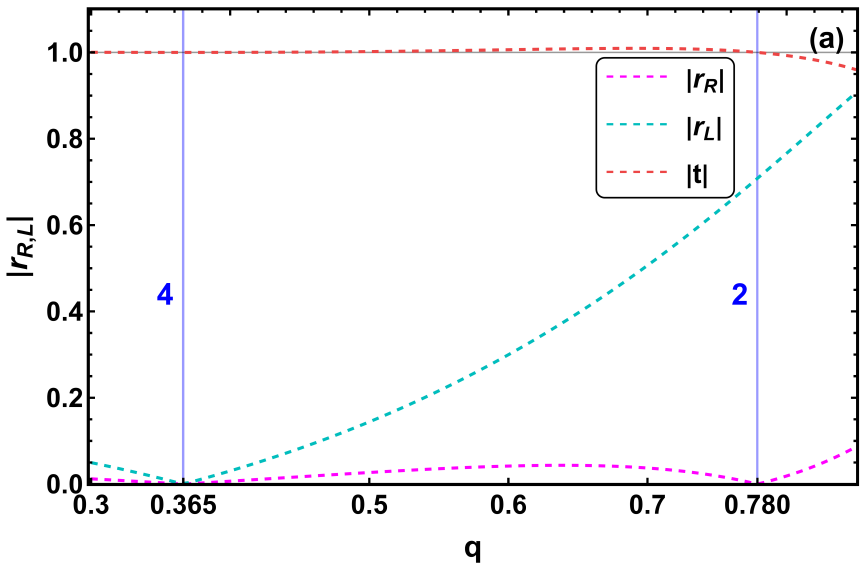


Figure 7. *Cont.*

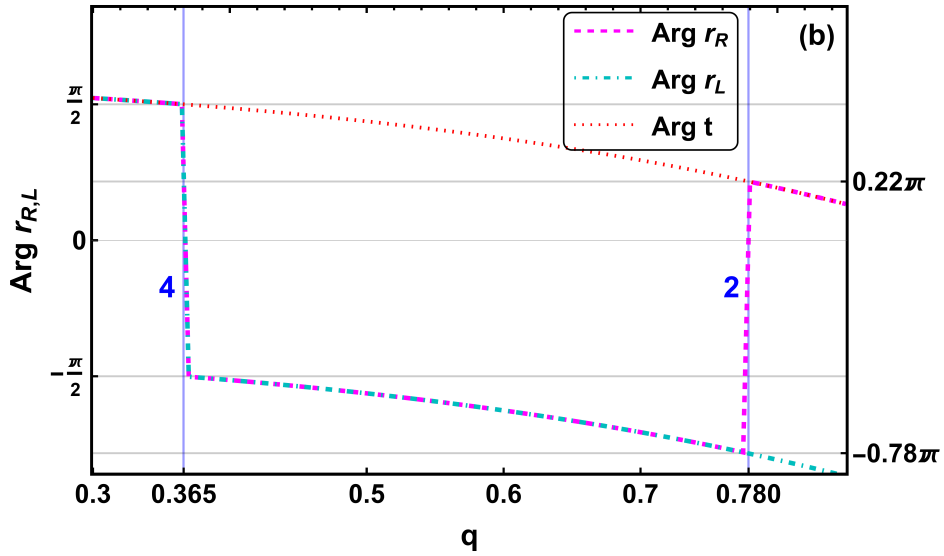


Figure 7. Moduli (**a**) and arguments (**b**) of the complex reflection r_R, r_L and transmission t amplitudes for the layer thickness $d = 75$ nm, $\varepsilon'' = 2$ and the number of unit cells $N = 5$.

4. Discussion and Conclusions

We have derived expressions for two types of nonparaxial TE-polarized Bessel beam's scattering matrices to investigate $\mathcal{PT}$ symmetry phase transitions in multilayer structures composed of alternating gain and loss layers of equal thickness. To comprehensively explore these systems, we have varied key parameters including the imaginary part of layers' permittivity ε'', layer thickness d, number of unit cells N, and normalized transverse wavenumber $q = \sin\theta$, which is determined by the half-cone angle of the propagating Bessel beam θ in the air surroundings (in the case of evanescent beams, the wavenumber $q > 1$.

We have demonstrated that the layer thickness d and the number of unit cells N have a similar effect on available $\mathcal{PT}$ symmetry transitions, as both scale the accumulated phase and provide resonance conditions. For the scattering matrix S_1, the increase in N results in the emergence of new regions with opposite $\mathcal{PT}$-symmetric phases in the parameter space, with distinct behaviors observed for even and odd numbers of layers. The difference depends on the specific choice of the thickness d. For the particular case of $d = 125$ nm, exceptional points in the space of q and ε'' appear only at $N = 2$. For the matrix S_2, however, increasing N leads to the appearance of additional eigenvalue degeneracy (diabolic) lines. We have conducted a comparative analysis of the transmittance T and reflectances R_L and R_R and associated reflectances' minima with the EP and diabolic degeneracy lines of the scattering matrix S_2. This identifies a $\mathcal{PT}$ symmetry phase transition when a minimum in a single reflection coefficient is observed and a diabolic line when both left and right reflectances vanish. Furthermore, we have analyzed the complex reflection and transmission coefficients to rigorously distinguish exceptional points from diabolic points, confirming that EPs correspond to unidirectional reflectionless scattering while DPs correspond to bidirectional reflectionless scattering.

The theoretical foundations of this research, specifically the integration of $\mathcal{PT}$ symmetry with evanescent structured light, fill a gap in non-Hermitian photonics. Owing to the translational invariance of the planar interfaces, the positions of exceptional and diabolic points of the Bessel beam are identical to those of a plane wave incident at the same angle. The derived scattering matrix formalism and the resulting $\mathcal{PT}$-symmetric phase diagrams, EPs, and DPs are universally preserved regardless of the order of the Bessel beam m, establishing a robust framework that extends conventional plane-wave models

to the domain of structured, nonparaxial, and evanescent light. It is well-established that operating non-Hermitian systems near an exceptional point yields exponentially enhanced sensitivity to local perturbations, surpassing the fundamental limits of conventional Hermitian sensors [36]. The framework presented in this manuscript can be directly applied to elevate sensing technologies. For instance, the recent advances in high-performance surface plasmon resonance sensing ground on hybrid periodic structures, such as arrayed resonant cavities combined with 2D metal–organic frameworks, to ensure signal homogeneity and enhance local hotspots [37]. Illuminating such extended periodic interfaces with non-diffracting evanescent Bessel beams offers a novel pathway to eliminate irregular hotspot distribution, ensuring robust excitation across the sensing area. Similarly, dynamically tunable metamaterials in the terahertz regime, such as Dirac semimetal AlCuFe quasicrystals, have recently enabled high-sensitivity multi-band absorption devices [38]. Embedding such platforms into a $\mathcal{PT}$-symmetric configuration and probing them with structured Bessel beams could leverage the extreme sensitivity of exceptional points to further enhance the Q-factor and refractive index sensitivity for multi-wavelength spectral analysis. While the fundamental concepts of reflectionless scattering modes and EP-enhanced sensing have been established in non-Hermitian systems [13,39], our work significantly extends this theoretical framework to the previously unaddressed domain of structured, nonparaxial, and evanescent Bessel beams. Furthermore, while exceptional points have been successfully demonstrated in experimental platforms such as microwave resonators [40] and optical fibers [41], our comprehensive scattering matrix formalism provides the essential theoretical toolkit required to upgrade these existing systems with structured light. The results of this work may pave the way for future $\mathcal{PT}$ symmetry research exploiting propagating and evanescent optical Bessel beams.

Author Contributions: Conceptualization, A.N.; methodology, A.N.; software, M.D.; validation, A.N.; investigation, M.D.; data curation, M.D.; writing—original draft preparation, M.D.; writing—review and editing, A.N.; visualization, M.D.; supervision, A.N. All authors have read and agreed to the published version of the manuscript.

Funding: The work is supported by the Belarusian Republican Foundation for Fundamental Research (Project No. F26RNF-106).

Data Availability Statement: The raw data supporting the conclusions of this article will be made available by the authors upon request.

Conflicts of Interest: The authors declare no conflicts of interest.

Abbreviations

The following abbreviations are used in this manuscript:

$\mathcal{PT}$	Parity-time
EP	Exceptional point
DP	Diabolical point

References

1. Bender, C.M.; Boettcher, S. Real Spectra in Non-Hermitian Hamiltonians Having $\mathcal{PT}$ Symmetry. *Phys. Rev. Lett.* **1998**, *80*, 5243–5246. [CrossRef]
2. Bender, C.M.; Brody, D.C.; Jones, H.F. Complex Extension of Quantum Mechanics. *Phys. Rev. Lett.* **2002**, *89*, 270401. [CrossRef] [PubMed]
3. Lin, Z.; Ramezani, H.; Eichelkraut, T.; Kottos, T.; Cao, H.; Christodoulides, D.N. Unidirectional Invisibility Induced by $\mathcal{PT}$-Symmetric Periodic Structures. *Phys. Rev. Lett.* **2011**, *106*, 213901. [CrossRef] [PubMed]
4. Ammari, H.; Davies, B.; Hiltunen, E.O.; Lee, H.; Yu, S. Exceptional Points in Parity–Time-Symmetric Subwavelength Metamaterials. *SIAM J. Math. Anal.* **2022**, *54*, 6223–6253. [CrossRef]

5. Chong, Y.D.; Ge, L.; Cao, H.; Stone, A.D. Coherent Perfect Absorbers: Time-Reversed Lasers. *Phys. Rev. Lett.* **2010**, *105*, 053901. [CrossRef] [PubMed]
6. Longhi, S. $\mathcal{PT}$-symmetric laser absorber. *Phys. Rev. A* **2010**, *82*, 031801. [CrossRef]
7. Chong, Y.D.; Ge, L.; Stone, A.D. $\mathcal{PT}$-Symmetry Breaking and Laser-Absorber Modes in Optical Scattering Systems. *Phys. Rev. Lett.* **2011**, *106*, 093902. [CrossRef] [PubMed]
8. Farhat, M.; Yang, M.; Ye, Z.; Chen, P.-Y. $\mathcal{PT}$-Symmetric Absorber-Laser Enables Electromagnetic Sensors with Unprecedented Sensitivity. *ACS Photonics* **2020**, *7*, 2080–2088. [CrossRef]
9. Alaee, R.; Christensen, J.; Kadic, M. Optical Pulling and Pushing Forces in Bilayer $\mathcal{PT}$-Symmetric Structures. *Phys. Rev. Appl.* **2018**, *9*, 014007. [CrossRef]
10. Novitsky, D.V. CPA-laser effect and exceptional points in $\mathcal{PT}$-symmetric multilayer structures. *J. Opt.* **2019**, *21*, 085101. [CrossRef]
11. Zhou, X.; Lin, X.; Xiao, Z.; Low, T.; Alù, A.; Zhang, B.; Sun, H. Controlling photonic spin Hall effect via exceptional points. *Phys. Rev. B* **2019**, *100*, 115429. [CrossRef]
12. Mostafazadeh, A. Scattering Theory and $\mathcal{PT}$-Symmetry. In *Parity-Time Symmetry and Its Applications*; Christodoulides, D., Yang, J., Eds.; Springer Tracts in Modern Physics 280; Springer: Singapore, 2018; pp. 75–121.
13. Sweeney, W.R.; Hsu, C.W.; Stone, A.D. Theory of reflectionless scattering modes. *Phys. Rev. A* **2020**, *102*, 063511. [CrossRef]
14. Dembowski, C.; Gräf, H.-D.; Harney, H.L.; Heine, A.; Heiss, W.D.; Rehfeld, H.; Richter, A. Experimental Observation of the Topological Structure of Exceptional Points. *Phys. Rev. Lett.* **2001**, *86*, 787–790. [CrossRef] [PubMed]
15. Ge, L.; Chong, Y.D.; Stone, A.D. Conservation relations and anisotropic transmission resonances in one-dimensional $\mathcal{PT}$-symmetric photonic heterostructures. *Phys. Rev. A* **2012**, *85*, 023802. [CrossRef]
16. Novitsky, D.V.; Shalin, A.S.; Redka, D.; Bobrovs, V.; Novitsky, A.V. Quasibound states in the continuum induced by $\mathcal{PT}$ symmetry breaking. *Phys. Rev. B* **2021**, *104*, 085126. [CrossRef]
17. Ramanovich, M.; Novitsky, A.; Novitsky, D.V. Mode Exchange and Phase Jumps at Exceptional Points in Anisotropy-Driven Layered Non-Hermitian Structures. *Photonics* **2026**, *13*, 201. [CrossRef]
18. Chen, Z.; He, H.; Li, H.; Li, M.; Kou, J.-L.; Lu, Y.-Q.; Xu, J.; Alù, A. Observation of parity-time symmetry for evanescent waves. *Commun. Phys.* **2024**, *7*, 339. [CrossRef]
19. Ruschin, S.; Leizer, A. Evanescent Bessel beams. *J. Opt. Soc. Am. A* **1998**, *15*, 1139–1143. [CrossRef]
20. Loran, F.; Mostafazadeh, A. Fundamental transfer matrix for electromagnetic waves, scattering by a planar collection of point scatterers, and anti-$\mathcal{PT}$-symmetry. *Phys. Rev. A* **2023**, *107*, 012203. [CrossRef]
21. Novitsky, A.; Lyakhov, D.; Michels, D.; Pavlov, A.A.; Shalin, A.S.; Novitsky, D.V. Unambiguous scattering matrix for non-Hermitian systems. *Phys. Rev. A* **2020**, *101*, 043834. [CrossRef]
22. Shramkova, O.V.; Tsironis, G.P. Scattering properties of $\mathcal{PT}$-symmetric layered periodic structures. *J. Opt.* **2016**, *18*, 105101. [CrossRef]
23. Pires, D.G.; Litchinitser, N.M.; Brandão, P.A. Scattering of partially coherent vortex beams by a $\mathcal{PT}$-symmetric dipole. *Opt. Express* **2021**, *29*, 15576–15586. [CrossRef] [PubMed]
24. Yang, M.; Zhang, H.-Q.; Liao, Y.-W.; Liu, Z.-H.; Zhou, Z.-W.; Zhou, X.-X.; Xu, J.-S.; Han, Y.-J.; Li, C.-F.; Guo, G.-C. Realization of exceptional points along a synthetic orbital angular momentum dimension. *Sci. Adv.* **2023**, *9*, eabp8943. [CrossRef] [PubMed]
25. Arfan, M.; Althobaiti, S.; Althobaiti, A.; Meglinski, I. Structured light scattering by a complex conjugate medium: The role of orbital angular momentum. *J. Quant. Spectrosc. Radiat. Transf.* **2026**, *363*, 110071. [CrossRef]
26. Xiao, L.; Wang, K.; Qu, D.; Gao, H.; Lin, Q.; Bian, Z.; Zhan, X.; Xue, P. Non-Hermitian physics in photonic systems. *Photonics Insights* **2025**, *4*, R09. [CrossRef]
27. Durnin, J. Exact solutions for nondiffracting beams. I. The scalar theory. *J. Opt. Soc. Am. A* **1987**, *4*, 651–654. [CrossRef]
28. Durnin, J.; Miceli, J.J., Jr.; Eberly, J.H. Diffraction-free beams. *Phys. Rev. Lett.* **1987**, *58*, 1499–1501. [CrossRef] [PubMed]
29. Rondón, I. Acoustic spin and orbital angular momentum using evanescent Bessel beams. *J. Phys. Commun.* **2021**, *5*, 085015. [CrossRef]
30. Bliokh, K.Y.; Nori, F. Spin and orbital angular momenta of acoustic beams. *Phys. Rev. B* **2019**, *99*, 174310. [CrossRef]
31. Rao, A.S. Illustrations of Bessel Beams in s-Polarization, p-Polarization, Transverse Polarization, and Longitudinal Polarization. *Photonics* **2023**, *10*, 1092. [CrossRef]
32. Novitsky, A.V. Intensity transformation of vector Bessel beams using a multilayer system. *Opt. Commun.* **2008**, *281*, 5310–5314. [CrossRef]
33. Szederkenyi, K.; Julien, C.; Lagarde, B.; Olevsko, I.; Salomon, A.; Oheim, M. Spatially resolved refractometry, fluorophore-concentration, axial-position, and orientational imaging using an evanescent Bessel beam. *EPJ Web Conf.* **2024**, *309*, 04023. [CrossRef]
34. Novitsky, A.V.; Novitsky, D.V. Change of the size of vector Bessel beam rings under reflection. *Opt. Commun.* **2008**, *281*, 2727–2734. [CrossRef]

35. Arfan, M.; Asif, M.; Althobaiti, S.; Althubiti, S.; Althobaiti, A.; Li, R.; Tang, H.; Yang, R. Scattering analysis and optical efficiencies of a complex conjugate medium (CCM) sphere illuminated by a non-diffracting linearly polarized Bessel beam. *Opt. Quantum Electron.* **2025**, *57*, 413. [CrossRef]
36. Budich, J.C.; Bergholtz, E.J. Non-Hermitian topological sensors. *Phys. Rev. Lett.* **2020**, *125*, 180403. [CrossRef] [PubMed]
37. Li, Y.; Liu, W.; Liu, R.; Gao, J.; Feng, J.; Xu, S.; Li, Z.; Jiang, S.; Du, X. 3D hybrid arrayed Ag/MOF multi-plasmon resonant cavity system for high-performance SPR sensing. *Opt. Laser Technol.* **2023**, *167*, 109825. [CrossRef]
38. Huang, J.; Cheng, S. Six-band high-sensitivity terahertz absorption device based on AlCuFe quasicrystals for sensing applications. *Phys. B Condens. Matter* **2026**, *741*, 419152. [CrossRef]
39. Ferise, C.; del Hougne, P.; Félix, S.; Pagneux, V.; Davy, M. Exceptional points of $\mathcal{PT}$-symmetric reflectionless states in complex scattering systems. *Phys. Rev. Lett.* **2022**, *128*, 203904. [CrossRef] [PubMed]
40. Wang, J.; Qi, X.; Yu, Y.; Wu, B.; Guo, Z.; Jiang, H.; Chen, H.; Sun, Y. Experimental observation of coherent perfect absorption in anti-parity-time-symmetric side-coupled microwave resonators. *Phys. Rev. A* **2026**, *113*, 063512. [CrossRef]
41. Bergman, A.; Duggan, R.; Sharma, K.; Tur, M.; Zadok, A.; Alù, A. Observation of anti-parity-time-symmetry, phase transitions and exceptional points in an optical fibre. *Nat. Commun.* **2021**, *12*, 486. [CrossRef] [PubMed]

Disclaimer/Publisher's Note: The statements, opinions and data contained in all publications are solely those of the individual author(s) and contributor(s) and not of MDPI and/or the editor(s). MDPI and/or the editor(s) disclaim responsibility for any injury to people or property resulting from any ideas, methods, instructions or products referred to in the content.